



Arisawa, D., Umetsu, Y., Yoshizawa, A., Hill, C., Eastoe, J., Guittard, F., Darmanin, T., & Sagisaka, M. (2021). Controlling water adhesion on superhydrophobic surfaces with bi-functional polymers. *Colloids and Surfaces A: Physicochemical and Engineering Aspects*, 616, [126307]. <https://doi.org/10.1016/j.colsurfa.2021.126307>

Peer reviewed version

License (if available):
CC BY-NC-ND

Link to published version (if available):
[10.1016/j.colsurfa.2021.126307](https://doi.org/10.1016/j.colsurfa.2021.126307)

[Link to publication record in Explore Bristol Research](#)
PDF-document

This is the author accepted manuscript (AAM). The final published version (version of record) is available online via Elsevier at <https://doi.org/10.1016/j.colsurfa.2021.126307>. Please refer to any applicable terms of use of the publisher.

University of Bristol - Explore Bristol Research

General rights

This document is made available in accordance with publisher policies. Please cite only the published version using the reference above. Full terms of use are available:
<http://www.bristol.ac.uk/red/research-policy/pure/user-guides/ebr-terms/>

Controlling water adhesion on superhydrophobic surfaces with bi-functional polymers

Daiki Arisawa^a, Yasushi Umetsu^a, Atsushi Yoshizawa^a, Christopher Hill^b, Julian Eastoe^b,
Frédéric Guittard^c, Thierry Darmanin^c, Masanobu Sagisaka^{a,*}

^a*Graduate School of Science and Technology, Hirosaki University, Bukyo-cho 3, Hirosaki,
Aomori, 0368561, Japan*

^b*School of Chemistry, University of Bristol, Cantock's Close, Bristol BS8 1TS, U.K.*

^c*Université Côte d'Azur, NICE Lab, 06200 Nice, France*

Corresponding Author

*E-mail sagisaka@hirosaki-u.ac.jp; FAX +81-172-39-3579 (M.S.)

Abstract

With an aim to control the surface hydrophobicity and water adhesion, as observed on various natural surfaces, novel 3,4-propylenedioxythiophene (ProDOT) monomers having one and two 3-trimethylsilylpropyl (TMS) groups were synthesized and subjected to electropolymerization to form surface coatings. The monomer ProDOT is employed owing to its tendency to form fibrous structures by electropolymerization [T. Darmanin, F. Guittard, *Mater. Chem. Phys.* 146 (2014) 6–11], whereas the TMS groups generate very low surface energies comparable to short chain fluorocarbons [N. M. Kovalchuk, et al., *Colloids Surfaces A* 604 (2020) 125277.]. It is shown that even though these two types of monomer lead to fibrous structures, the dimensions of the fibers as well as the wetting properties are different. The monomer with only a single TMS group (ProDOTSiMe₃) generates extremely long nanofibers with only low surface roughness. The resulting surfaces have extremely high apparent contact angles (θ_w) up to 141.7° and strong water adhesion, similar to rose petals or gecko feet. On the other hand, the analogue with two TMS groups (ProDOT(SiMe₃)₂) forms short nanofibers but with extremely high surface roughness. The resulting surfaces are superhydrophobic with $\theta_w > 160^\circ$ and ultra-low water adhesion (hysteresis and sliding angles $< 1^\circ$), similar to lotus leaves. These results point to interesting applications offering control over water adhesion whilst maintaining high hydrophobicity.

Keywords: Trimethyl silyl group, superhydrophobicity, parahydrophobicity, water adhesion, electropolymerization, surface roughness

1. Introduction

The observation of exceptional wetting properties of natural surfaces (lotus leaves, rose petals, gecko feet etc.) has stimulated significant interest in the scientific community seeking to understand the origins of these phenomena and use them in practical applications [1-6]. Indeed, nature exploits surface wettability to reduce/increase contact with water in various intriguing ways, for example, to walk on water surfaces or to see clearly in foggy environments. All these effects are implicitly linked to the specific surface chemistry and surface structuring as previously noted by Wenzel [7] and Cassie-Baxter [8], and intensely studied by other research groups [9-14]. Namely, wettability on a solid surface is explained with the equations of Wenzel [7] ($\cos \theta = r \cos \theta^Y$, where r is a roughness parameter and θ^Y is the Young's angle) and Cassie-Baxter [8] ($\cos \theta = f \cos \theta^Y + f - 1$, where f is the solid fraction and $(1 - f)$ is the air fraction). However, the Wenzel and Cassie-Baxter equations are dependent on θ^Y , which corresponds to the apparent contact angle of a liquid on a smooth, homogeneous, rigid, insoluble, and non-reactive solid surface, as described by Marmur [10]. In particular, superhydrophobic properties have been reported when the apparent contact angle (θ_w) is above 150° with very *low* water adhesion: this combination of properties is typically obtained when the volume fraction of air between the substrate and water is significant (lotus leaves). In contrast, other species are able to capture and transport water droplets thanks to both high θ_w and *high* water adhesion, such surfaces are referred to a parahydrophobic, as described by Marmur [15].

Controlling the surface hydrophobicity and water adhesion is possible via several different methods. For example, surfaces with different surface structures and surface energies can be prepared by multiple methods (electropolymerization, nanoparticles coatings, laser treatments, plasma treatments...) [16-18]. Otherwise, if the surface is sensitive to stimuli, the surface structures and surface energies can be adjusted after formation [19-21].

There are some promising applications that utilize superhydrophobic surfaces and water adhesive properties. For example, gas-transportation in aqueous media [12,13] and water-oil separation [6] employ superhydrophobic/low water adhesive surfaces, and water harvesting systems [22] make use of parahydrophobic surfaces. A range of different biological systems show how fundamental the control of water adhesion is in nature. Hence, it is of interest to learn how to replicate these properties by controlling both the surface chemistry and surface structure. In earlier papers, the water adhesion and hydrophobicity of various material surfaces were successfully tuned by laser irradiation, long-chain fatty acid modification, temperature control, and/or polymer hydrogel formation [23-25]. Conducting polymers are also interesting and useful because they can generate various structured materials by self-assembly. For example, the polymerization of aniline has been extensively studied [26]: owing to high intra- and intermolecular interactions such as hydrogen bonding, hydrophobic and π -stacking interactions, various assemblies such as nanofibers (1D growth), nanosheets (2D growth) or flower-like and urchin-like structures (3D growth) are possible depending on the polymerization conditions. Using electropolymerization, the monomer 3,4-propylenedioxythiophene (ProDOT) is also known to form nanofibers. As such ProDOT serves as a flexible template for modification with different substituents offering a broad tunability of both surface structures and wetting properties [27-31]. In particular, when the substituents are orthogonal across the ProDOT moiety [32-34] long polymer chains and good quality fibers structures may be generated, and in this respect both hydrocarbon and chains and fluoroalkyl chains have been studied [35-38]. Here, we report for the first time the formation of nanofibrous structures from two kinds of ProDOT monomer, substituted with either one or two trimethylsilyl (TMS) groups. The investigated monomers named ProDOTSiMe₃ and ProDOT(SiMe₃)₂ are represented in **Figure 1**.

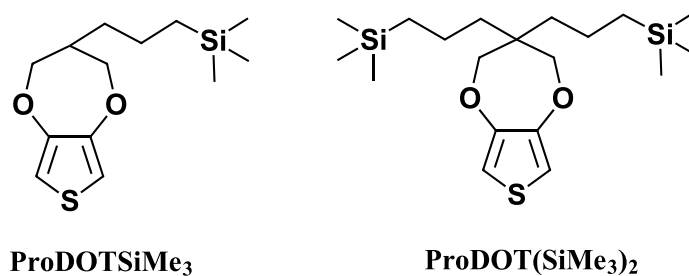


Figure 1. Structures of thiophene monomers having trimethylsilyl groups

In earlier studies, surfactants having TMS-terminated tails were found to generate very low surface energies (surface tensions), and comparable to short fluorocarbons in water (the limiting aqueous surface tension is 22.8 mN/m for the double TMS-chain terminated surfactant AOTSiC) [39]. As an example application of low surface energy surfactants, superspreading of aqueous solution on polyvinylidene difluoride (PVDF) surface was demonstrated by using the TMS surfactant [40,41]. Therefore, combining these two functions together, polymer films prepared with TMS-bearing ProDOTSiMe₃ and ProDOT(SiMe₃)₂ thiophene monomers are expected to exhibit superhydrophobicity as well as oleophobicity as found uniquely with fluoro-polymers [41,42]. The concept is explored here, and it is observed that electropolymerization of ProDOTSiMe₃ and ProDOT(SiMe₃)₂ give rise to notably different surface structures and properties, this leads to very different surface roughnesses and adhesion of water droplets to these functionalized surfaces. More precisely, ProDOTSiMe₃ bearing a single TMS group generates extremely long nanofibers with only low surface roughness, resulting in an extremely high apparent water contact angle (θ_w) up to 141.7° and strong water adhesion, similar to rose petals or gecko feet. On the other hand, ProDOT(SiMe₃)₂ with two TMS groups forms short nanofibers but with extremely high surface roughness. These functionalized surfaces exhibit superhydrophobic ($\theta_w > 160^\circ$) as well as ultra-low water adhesion (hysteresis and sliding angles $< 1^\circ$), similar to lotus leaves. By comparing these data with results reported in earlier papers, critical values in the

roughness parameter (Ra) and total carbon number of monomer substituents for Lotus and Petal effects, as well as parahydrophobicity are presented.

2. Experimental Section

2.1. Materials

ProDOT monomers substituted with either one or two trimethylsilyl (TMS) groups (ProDOTSiMe₃ and ProDOT(SiMe₃)₂) were synthesized and purified as shown in Supplementary data. Sodium bicarbonate (purity 99.0%), anhydrous tetrahydrofuran (purity 99.5%), sodium hydride (60%, dispersion in paraffin liquid), 6 mol/L sodium hydroxide, *p*-toluenesulfonic acid monohydrate (purity 99.0%), sulfuric acid (purity 95%), sodium chloride (purity 99.5%), 0.5 mol/L hydrochloric acid, sodium sulfate (purity 99.0 %), sodium iodide (purity 99.0 %), acetone (purity 99.5%) were purchased from FUJIFILM Wako Pure Chemical. Diethylmalonate (purity 99.0%), LiAlH₄ (10%, dispersion in THF), 3,4-dimethoxythiophene (purity 98%), potassium sodium L-(+)- tartrate tetrahydrate (purity >98.0%), sodium *tert*-butoxide (purity > 98%) were obtained from Tokyo Chemical Industry. Phosphorus tribromide (purity 99%, Sigma-Aldrich), 3-(trimethylsilyl)propan-1-ol (purity 97.0%, Sigma-Aldrich), chloropropyltrimethylsilane (purity 95~100%, Gelest, Inc.) were also used without further purification. Ultrapure water with a resistivity of 18.2 MΩ cm was obtained from a Millipore Milli-Q Plus system.

2.2. Electrochemical data

Electrochemical polymerizations were performed using a potentiostat (Metrohm Autolab) equipped with a three-electrode system fitted with a gold plate (2 cm²) as the working electrode, a carbon-rod as the counter electrode and a saturated calomel electrode (SCE) as the reference electrode. The electrochemical cell was first filled with 10 mL of anhydrous acetonitrile containing 0.1 mol L⁻¹ of tetrabutylammonium perchlorate (Bu₄NClO₄) as the electrolyte as well as 0.01 M of monomer. After determination of the oxidation potential ($E^{\text{ox}} = 1.48 \text{ V vs SCE}$) for each synthesized monomer, electropolymerizations were

performed under potentiodynamic conditions via cyclic voltammetry at a scan rate of 20 mV s⁻¹. The total number of scans was varied (1, 3 and 5) in order to study polymer growth. After electrodeposition, the substrates were washed three times in acetonitrile.

2.3. Surface characterization

Surface hydrophobicity was characterized by goniometry using a DSA30 goniometer (Bruker) and the “Drop Shape Analysis System” software. Water droplets (2 μL) were deposited onto surfaces and the apparent contact angles (θ_w) were determined. Each data point presented reflects a mean of five measurements ($n = 5$). For dynamic contact angles, after deposition of a water droplet, the substrate was inclined until the droplet moved. The maximum inclination angle is named sliding angle (α). The advancing and receding contact angles are taken just before the droplet moves. In case the droplets do not move, even with an inclination of 90°, the substrates are considered sticky and can be described as parahydrophobic. Surface morphology was investigated via scanning electron microscopy (SEM) using a JEOL 6700F microscope. The arithmetic (R_a) and quadratic (R_q) roughness were obtained with a WYKO NT1100 optical profiling (Bruker). We used an objective 20X, field of view 0.5X and white light vertical scanning Interferometry (VSI).

3. Results and Discussion

3.1. Formation of coatings by electropolymerization

First, the monomer oxidation potential E^{ox} in $\text{Bu}_4\text{NClO}_4/\text{acetonitrile}$ was determined at 1.48 V vs SCE for the two monomers. Next, the polymers were deposited under cyclic voltammogram conditions from -1 V to E^{ox} at a scan rate of 20 mV s^{-1} and with different numbers of scans (1, 3, 5). Here, in order to study the effect of the amount of electrodeposited polymer, it was chosen to keep the scan rate constant and to vary the number of scans. Representative cyclic voltammograms are presented in **Figure 2**, showing oxidation and reduction conducting polymer peaks clearly present. In addition, the superposition after each scan indicates essentially negligible steric hindrance owing to the TMS substituents. Peaks are present at 0.33 V during the forward scans (oxidation) and 0.13 V during the reverse scans (reduction) for ProDOTSiMe₃. On the other hand, these features are seen at 0.46 V and 0.29 V for ProDOT(SiMe₃)₂, respectively. This increase in potential is likely due to shortening of the polymer chain when two substituents are present.

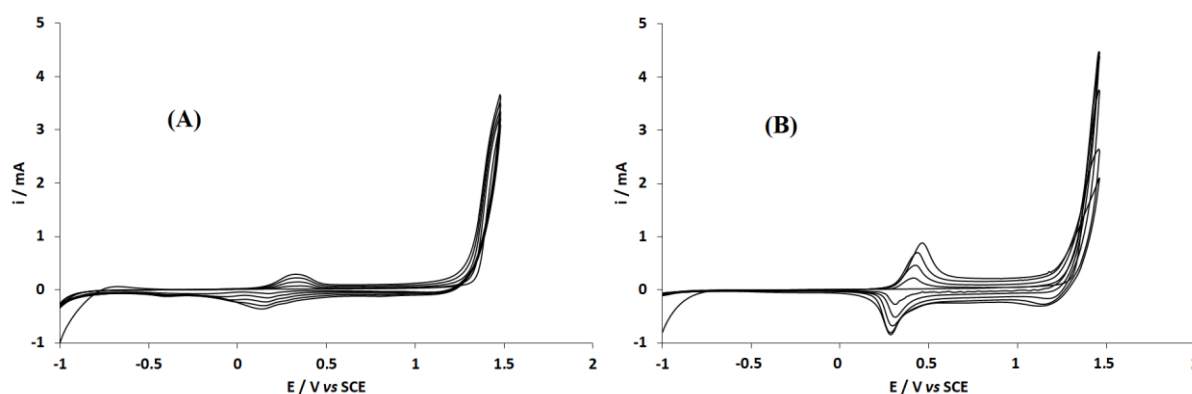


Figure 2. Cyclic voltammograms (5 scans) of ProDOTSiMe₃ (A) and ProDOT(SiMe₃)₂ (B) in acetonitrile with Bu_4NClO_4 as electrolyte. Scan rate: 20 mV s^{-1} .

3.2. Characterization of the nanofibrous surfaces

The surface morphology after electrodeposition via cyclic voltammetry (1, 3 and 5 scans) of the two monomers in acetonitrile is highlighted in **Figures 3** and **4**. From these images it is clear that the electropolymerization of these two monomers leads to nanofibrous structures as generally found for ProDOT-based monomers [27-29]. The fibrous structures become increasingly noticeable, especially from 3 deposition scans. More precisely, ProDOTSiMe₃ forms extremely long fibers leading to porous surfaces but their surface roughness is not very high. In contrast, ProDOT(SiMe₃)₂ forms quite short nanofibrous structures with higher surface roughness, especially after 3 deposition scans (**Figure 4** and **Table 1**). When a polymer prepared by electrodeposition is structured as nanofibers, a larger scan number increases the number, diameter, and/or length of fibers. As seen in figure 4, fibers of ProDOT(SiMe₃)₂ tend to grow vertically toward the surface, in contrast with those for ProDOTSiMe₃ which grow laterally. In addition to the direction, fibers were found to grow in highly branched patterns like rose thorns. The significant increase in roughness from 1 scan to 3 scans for ProDOT(SiMe₃)₂ could be obtained by the growth direction and the hyperbranching of fibers.

Interestingly, the wetting properties of these two prepared surfaces are also clearly different. The surfaces obtained from ProDOTSiMe₃ are parahydrophobic [15] and display the highest $\theta_w = 141.7^\circ$ after 3 deposition scans (**Table 1**). Moreover, all these surfaces also have a very strong water adhesion. As shown in **Figure 5**, water droplets placed on them remained stuck even after tilting the substrate up to 90°; this kind of adhesion is observed on rose petals for example. Initially, the water droplets are in intermediate states between Wenzel and Cassie-Baxter states, whereas the surfaces obtained after 3 deposition scans are closer to the Cassie-Baxter, even though the water adhesion remains extremely high. These surfaces are very interesting and could be used in water harvesting systems, where it is important to

have both high hydrophobicity and high water adhesion in order to both capture water droplets and induce their motion when the droplet size becomes critical [22, 42-45 43-46].

Interestingly, water contact angle decreased with deposition scans from 3 to 5 with the ProDOTSiMe₃. As seen in Figure 3, the larger scan number increased not only roughness (*Ra* and *Rq*) but also the fiber diameter for ProDOTSiMe₃. Forming a larger fiber diameter also results in a lower number density of fibers and a wider interfibrillar distance as shown in Fig. 3. Such a surface tends to lead a deeper water intrusion in interfibrillar spaces, namely to prefer a Wenzel state rather than a Cassie-Baxter state. A deeper water intrusion to a rough surface makes a larger *f* value in Cassie-Baxter equation, $\cos \theta = f \cos \theta_Y + f - 1$ where *f* is the solid fraction and (*1 - f*) is the air fraction, resulting in the smaller water contact angle as found at 5th scan for ProDOTSiMe₃.

The surfaces obtained from ProDOT(SiMe₃)₂ are clearly superhydrophobic with $\theta_w > 160^\circ$ and ultra low-adhesion (hysteresis and sliding angles $< 1^\circ$). The water adhesion is so low that it is extremely difficult to deposit water droplets on these surfaces (**Figure 5**). The behavior of water droplets clearly suggests a Cassie-Baxter state. The surfaces are superhydrophobic even after one deposition scan indicating that it is not necessary to have high surface roughness. Hence, it was decided to analyze the effect of the number of deposition scans because usually after one scan surface roughness increases with the number of scans especially between 1 and 3 scans. However, it is known that there is no direct relationship between surface roughness and the apparent contact angles, and to reach the Cassie-Baxter state with ultra-low adhesion it is preferable to have surface structures able to trap a high amount of air between the droplet and the rough surface. This is why, here, with ProDOT(SiMe₃)₂ ultra-low adhesion is observed even after one scan, whereas the surface has relatively low (*Ra* = 76 nm). These surfaces are fibrous but with double scale roughness (micro/nano) as observed on lotus leaves. Moreover, the dimensions of the nanofibers are

much lower with ProDOT(SiMe₃)₂, as compared to the non-functionalized polymer. The shorter fibrous structures can be explained by the higher solubility of ProDOT(SiMe₃)₂ polymers because the formation of fibrous structures needs some time to induce a mono-directional growth (long fibrous structures) [10]. Different dimensions of fibrous structures have already been reported comparing surfaces electrodeposited from 3,4-ethylenedioxyppyrole (EDOP) and 3,4-propylenedioxyppyrole (ProDOP) but with the same substituent (C₄F₉) [46 47].

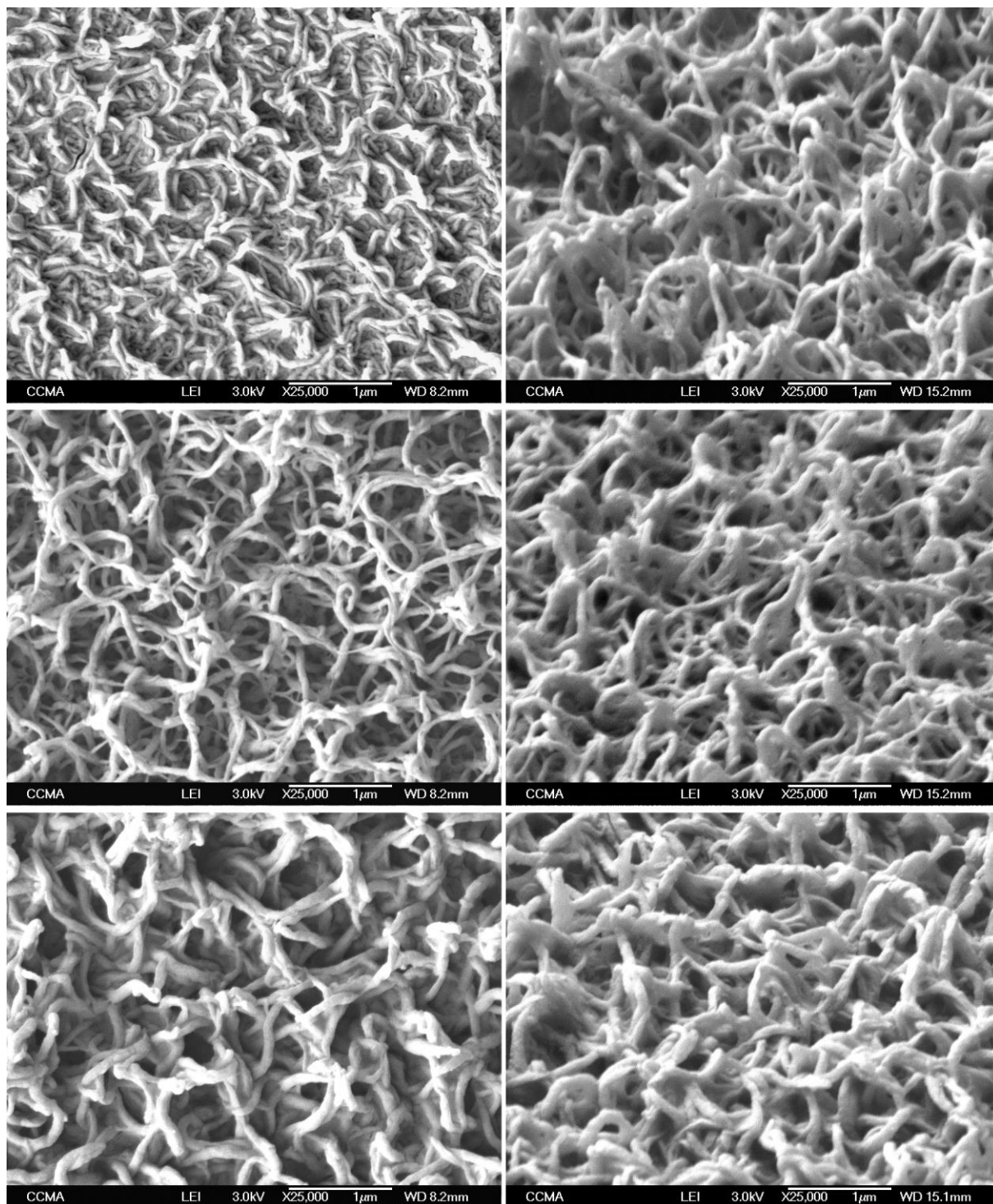


Figure 3. SEM images of polymer surfaces obtained from ProDOTSiMe₃ via cyclic voltammetry (1, 3 and 5 scans from top to bottom) without (left hand column) and with (right column) substrate inclination.

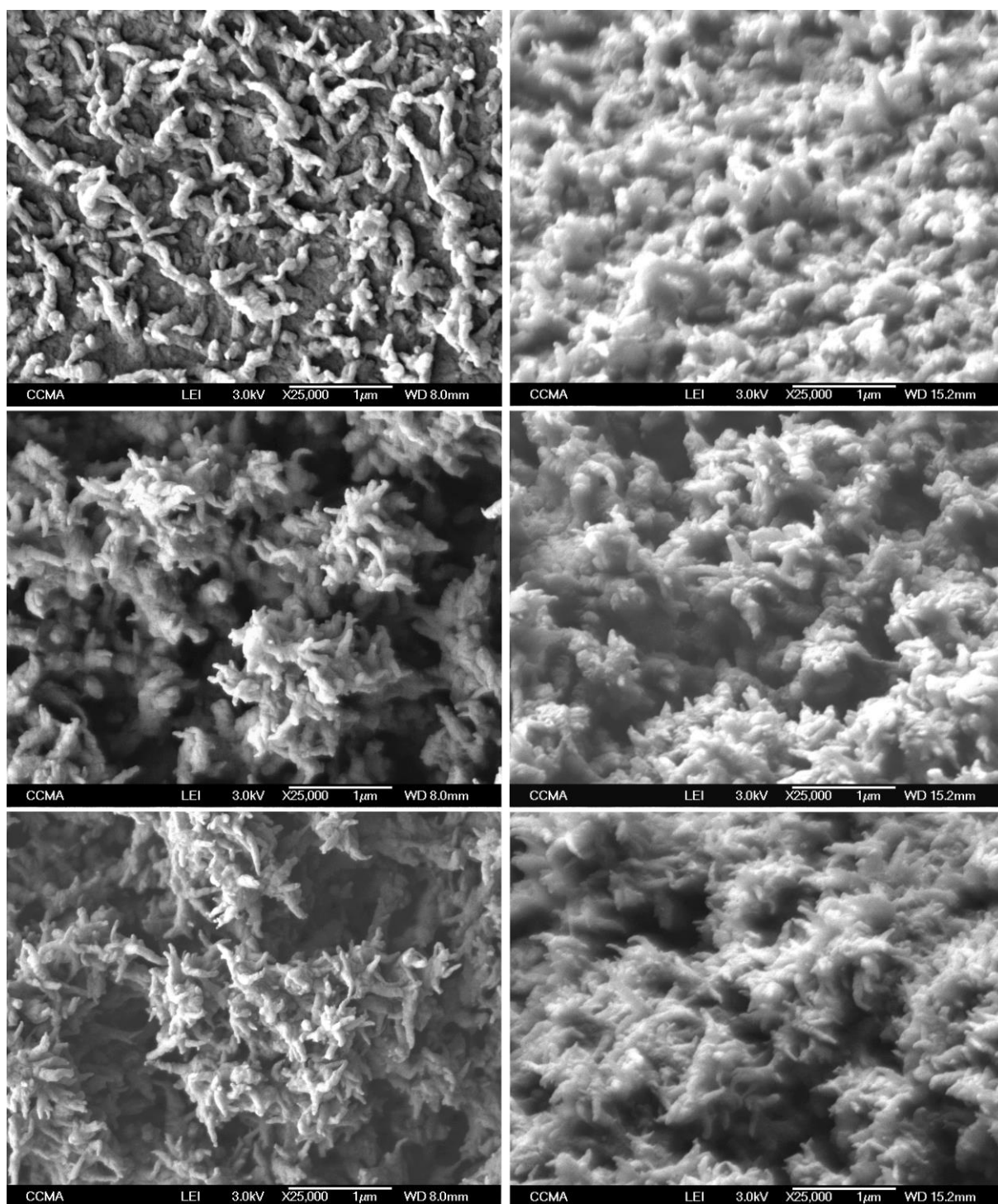


Figure 4. SEM images of polymer surfaces obtained from ProDOT(SiMe_3)₂ via cyclic voltammetry (1, 3 and 5 scans from top to bottom) without (left hand column) and with (right column) substrate inclination.

Table 1. Wettability data and arithmetic (R_a) and quadratic (R_q) surface roughness for the two polymers.

Monomer	Number of scans	R_a [nm]	R_q [nm]	θ_w [deg]	θ_{diiodo} [deg]	θ_{hexa} [deg]
ProDOTSiMe ₃	1	38 ± 10	49 ± 15	120.9 ± 2.4	48.9 ± 1.5	0
	3	112 ± 18	140 ± 21	141.7 ± 5.4	35.5 ± 4.3	0
	5	215 ± 27	280 ± 35	130.6 ± 1.7	30.5 ± 1.6	0
ProDOT(SiMe ₃) ₂	1	76 ± 8	90 ± 7	160.6 ± 2.0	69.6 ± 4.0	0
	3	2000 ± 150	3700 ± 250	163.4 ± 1.0	48.4 ± 5.7	0
	5	1250 ± 70	1920 ± 100	163.5 ± 1.3	34.7 ± 4.8	0



Figure 5. Picture of a water droplet placed on a substrate obtained from ProDOTSiMe₃ (left) and ProDOT(SiMe₃)₂ (right) via cyclic voltammetry (3 scans), and inclined at 90°.

3.3. Effects of substituent carbon number and branching on water contact angle and morphology

The findings for ProDOTSiMe₃ and ProDOT(SiMe₃)₂ are compared with previous results reported in the literature using ProDOT derivatives (**Table 2**) [28-38]. Indeed, various substituents including linear or branched alkyl chains, fluorinated chains as well as aromatic groups have been studied. To clarify the effects of substituents on hydrophobicity of the electrodeposited polymer films, θ_w of the electrodeposited polymers was plotted as a function of total carbon number in monomer substituents ($N_{c,total}$) [28-38] in **Figure 5**. Hereafter, results and discussion are focused on the data collected after three deposition scans, which results in the best performance for hydrophobicity, as commonly obtained in earlier papers [28-38] as well as this study. The effects of main chain length and branching factor [47-48] of the substituents were also investigated (supplementary material) but the effects are less clear compared with **Figure 6**.

In the case of nonfluorinated substituents, θ_w , which is a measure of hydrophobicity of the polymer film, was found to increase with $N_{c,total}$ up to 8, maintaining a constant $\sim 160^\circ$ being almost independent of chain branching. Generation of Petal and Lotus effects strongly depends on $N_{c,total}$, and those properties appeared at $N_{c,total} < 8$ and > 8 , respectively. On the other hand, higher F-content monomers tend to form spherical rather than fibrous structures and to produce smoother polymer surfaces, likely caused by stronger oleo-phobicity of the monomers towards the organic solvent. For these TMS-substituent monomers, the data for the single TMS-containing (ProDOTSiMe₃) followed the same trend of θ_w vs $N_{c,total}$ as for other nonfluorinated ProDOT families, and did not show any effect of the TMS group. However, the effect of TMS became clearer when two groups were employed in the monomer, producing the highest θ_w value ($163.4 \pm 1.0^\circ$) with ultralow water adhesion. In summary, even though fibrous structures were obtained with many of ProDOT compounds, this paper is the

first to report ultra-low water adhesion in addition to superhydrophobicity, and this combination of properties was obtained with TMS substituents in the ProDOT monomers.

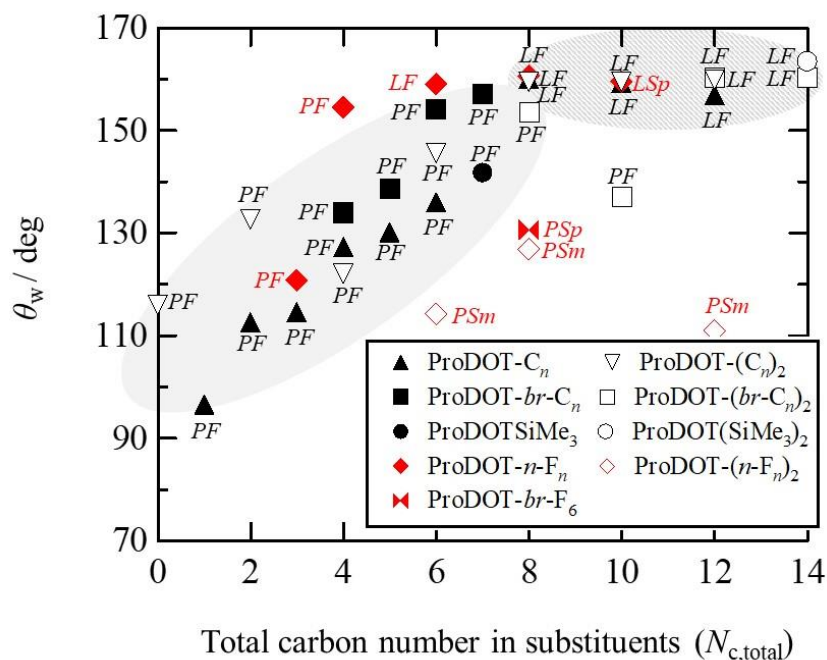
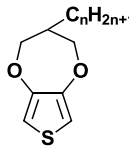
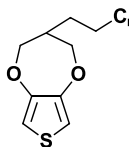
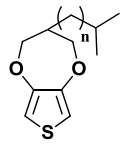
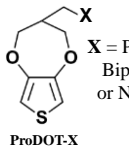
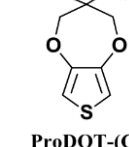
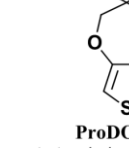
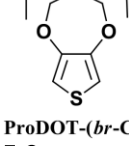
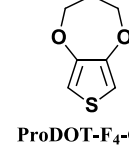
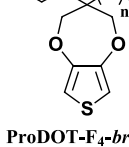


Figure 6. Relationship between θ_w and total carbon number in substituents of monomers for ProDOTSiMe₃, ProDOT(SiMe₃)₂ and ProDOT series reported in earlier papers [28-38]. All data are for three electrodeposition scans. The capital letters in each symbol mean P: Petal effect, L: Lotus effect, F: Fibrous structure, Sp: Spherical structure, and Sm: Smooth surface. Red/black and closed/open symbols mean fluorinated/nonfluorinated and single-chain/double-chain monomer, respectively.

Table 2. Surface structure and wetting properties reported in the literature for electropolymerization of various ProDOT derivatives [28-38].

Monomer	Surface structures	Contact angles	Water adhesion
 <p>ProDOT-C_n</p>	[35] $n = 1-8$: fibrous $190 < Ra < 1050$ nm $267 < Rq < 1390$ nm	$96.5 < \theta_w < 160.0^\circ$ θ_{diiodo}^* θ_{hexa}^*	$n = 1-6$: sticky $n > 8$: $5 < H < 35$
 <p>ProDOT-F_n</p>	[36] $n = 1-6$: fibrous $n = 8$: spheres $182 < Ra < 720$ nm $235 < Rq < 900$ nm	$114.2 < \theta_w < 159.5^\circ$ $63.1 < \theta_{\text{diiodo}} < 136.7^\circ$ $0 < \theta_{\text{hexa}} < 78.8^\circ$	$n = 1$: sticky $n = 2-8$: $3 < H < 10$
 <p>ProDOT-br-C_n</p>	[31] $n = 1-4$: fibrous Ra^* Rq^*	$132.0 < \theta_w < 157.0^\circ$ θ_{diiodo}^* θ_{hexa}^*	$n = 1-4$: sticky
 <p>ProDOT-X</p>	[28] X = Ph: fibrous X = BiPh, NaPh: spheres $375 < Ra < 945$ nm $490 < Rq < 1075$ nm	$134.5 < \theta_w < 159.1$ θ_{diiodo}^* θ_{hexa}^*	X = Ph: sticky X = BiPh, NaPh: $2 < H < 3$
 <p>ProDOT-(C_n)₂</p>	[32,34,37] $n = 1-6$: fibrous $40 < Ra < 485$ nm $73 < Rq < 612$ nm	$121.4 < \theta_w < 160.0^\circ$ θ_{diiodo}^* θ_{hexa}^*	$n = 1-3$: sticky $n = 4-6$: $7 < H < 29$
 <p>ProDOT-(F_n)₂</p>	[36] $n = 1-4$: smooth $52 < Ra < 61$ nm $66 < Rq < 81$ nm	$110.9 < \theta_w < 126.8^\circ$ $63.1 < \theta_{\text{diiodo}} < 110.6^\circ$ $0 < \theta_{\text{hexa}} < 73.7^\circ$	$n = 1-4$: sticky
 <p>ProDOT-(F_n)₂</p>	[30] $n = 1-4$: fibrous Ra^* Rq^*	$136.8 < \theta_w < 160.0^\circ$ θ_{diiodo}^* θ_{hexa}^*	$n = 1-2$: sticky $n = 3-4$: $5 < H < 6$
 <p>ProDOT-(br-C_n)₂</p>	[38] $n = 2$: fibrous $n = 4-6$: sheets Ra^* Rq^*	$139.0 < \theta_w < 160.4^\circ$ $112.3 < \theta_{\text{diiodo}} < 136.0^\circ$ $61.9 < \theta_{\text{hexa}} < 74.2^\circ$	$n = 2$: $H < 1$ $n = 4-6$: sticky
 <p>ProDOT-F₄-C_n</p>	[29] $n = 1-4$: sheets $130 < Ra < 270$ nm $180 < Rq < 400$ nm	$139.1 < \theta_w < 149.1^\circ$ $100.6 < \theta_{\text{diiodo}} < 111.1^\circ$ $70.0 < \theta_{\text{hexa}} < 74.5^\circ$	$n = 1-4$: sticky

* = not given

Further examinations focused on how roughness in these electrodeposited polymer films affects water contact angles. **Figure 7** shows the relationship between $(\theta_w - \theta_w^{\text{Smooth}})$ and Ra for the ProDOT series reported in earlier papers [28-38]. θ_w^{Smooth} values are water contact angles on smooth polymer film surfaces ($Ra < 10$ nm) [28-38], playing the role of θ^Y in the Wenzel and Cassie-Baxter equations [7,8]. As shown in the gray region of in **Figure 7**, larger roughness Ra lead to larger $(\theta_w - \theta_w^{\text{Smooth}})$ values according to both Wenzel and Cassie-Baxter theories. However, increasing Ra to over ~ 400 nm did not make $\theta_w - \theta_w^{\text{Smooth}}$ any larger due to the water contact angle already being $\sim 160^\circ$.

Looking at Lotus and Petal effects in Figure 7, the boundary between both effects was found to be at $Ra \sim 290$ nm. In the case of ProDOTSiMe₃, the Ra value was 112 nm and smaller than the boundary, resulting in the Petal effect, on the other hand, ProDOT(SiMe₃)₂ produced the largest $Ra \sim 2000$ nm. Hence, ProDOT(SiMe₃)₂ may amplify the Lotus effect the most and result in the highest θ_w . It is also interesting to note that non-fluorinated ProDOT series with a larger $N_{c,\text{total}}$ give a larger roughness Ra , and that to achieve $Ra > 290$ nm to generate the Lotus effect requires $N_{c,\text{total}} \geq 8$.

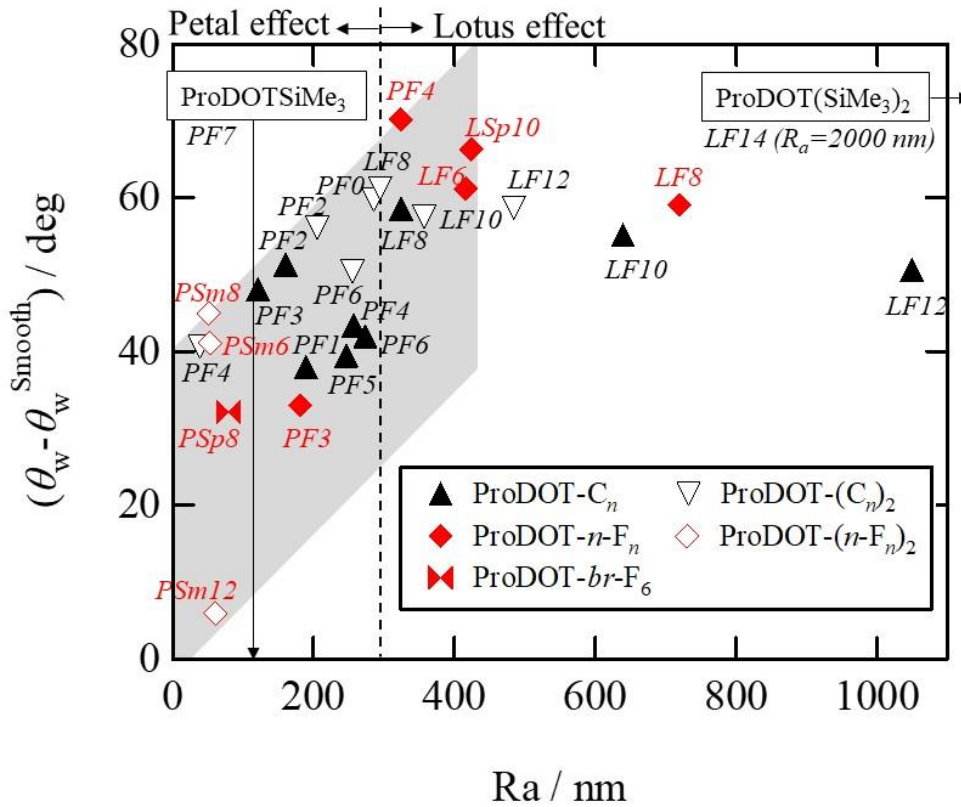


Figure 7. Relationship between $(\theta_w - \theta_w^{\text{Smooth}})$ and Ra for ProDOT series reported in earlier papers [28-38]. θ_w^{Smooth} is water contact angle on a smooth surface ($Ra < 10$ nm) of polymer films. All the data is for three electrodeposition scans. The capital letters in each symbol mean P: Petal effect, L: Lotus effect, F: Fibrous structure, Sp: Spherical structure, and Sm: Smooth surface. Red/black and closed/open symbols mean fluorinated/nonfluorinated and single-chain/double-chain monomer, respectively. The numbers following the capital letters are total C-numbers in the monomer substituents.

To clarify the effect of the roughness parameter (or air fraction) on θ_w , the relationship between $\cos \theta_w$ and $\cos \theta_w^{\text{Smooth}}$ was examined, as shown in **Figure 8**. The solid line in the graph displayed a linear function fitted to the data for ProDOT- C_n having Ra values of 122-274 nm. The function has a gradient of 0.792 and intercept -0.667, relating to f (or r in Wenzel equation [7]) and $f - 1$, respectively [8]. The different f values, 0.792 and 0.333 obtained from the gradient and the intercept imply water droplets on electrodeposited ProDOT- C_n polymer films are intermediate between Wenzel and Cassie-Baxter states [7,8] containing air fractions of 0.333-0.792. The Lotus effect was found in the gray region, this clearly shows that $\cos \theta_w^{\text{Smooth}} < 0$ (or $\theta_w^{\text{Smooth}} > 90^\circ$) as well as $Ra > 290$ nm are needed to generate the Lotus effect (**Figure 7**).

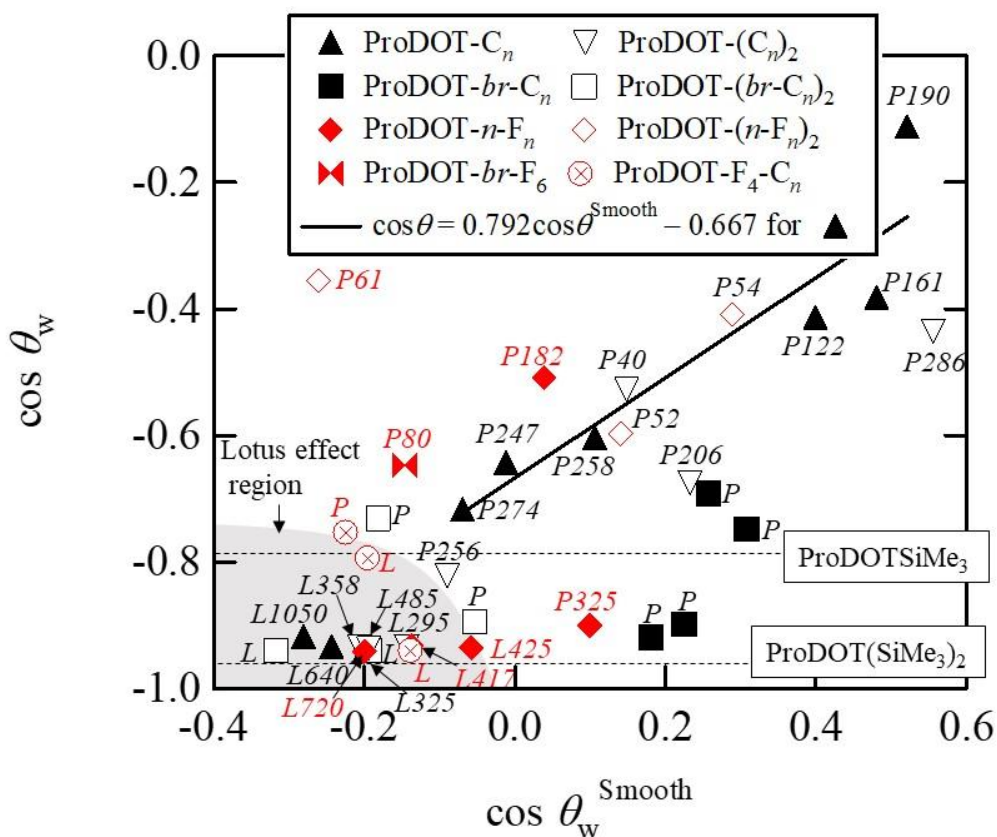


Figure 8. Relationship between $\cos \theta_w$ and $\cos \theta_w^{\text{Smooth}}$ for ProDOT series reported in earlier papers [28-38]. All the data is for three electrodeposition scans. The capital letters in each symbol mean P: Petal effect and L: Lotus effect. Red/black and closed/open symbols mean fluorinated/nonfluorinated and single-chain/di-chain monomer, respectively. The numbers following the capital letters are the Ra values.

4. Conclusions

It is of fundamental interest to learn how to control water adhesion. Here, it was demonstrated that control over nanofibrous surface structure can either lead to strong water adhesion (Petal effect) or ultra-low water adhesion (Lotus effect). More precisely, films of electropolymerized thiophene monomers (ProDOTSiMe₃ and ProDOT(SiMe₃)₂) having single and double TMS-terminated propyl constituents respectively, have been studied. Hydrophobicity and surface morphology of electrodeposited polymer films of these two monomers were compared with those from previous literature for a wider ProDOT series, having substituents of straight/branched fluorocarbons and hydrocarbons [28-38]. The following interesting findings (1)-(3) were obtained.

(1) ProDOTSiMe₃, having a single TMS-terminated propyl substituent, generated polymer films with tangled nanofibers, exhibiting water contact angles 120-142° and strong water adhesion (Petal effect). The films are identified to be intermediate between Wenzel and Cassie-Baxter states, and promising for water harvesting systems.

(2) Adding one more TMS-terminal substituent to the monomer, in ProDOT(SiMe₃)₂, made the nanofibers shorter, stand on end, and drastically increased roughness of the polymer films. For example, the *Ra* and *Rq* values for three deposition scans increased up by 20 times over the original ProDOTSiMe₃. As the result, the films for ProDOT(SiMe₃)₂ displayed ultra-low water adhesion (Lotus effect), Cassie-Baxter states, and achieved the highest superhydrophobicity in the ProDOT series, as indicated by water contact angles of ~163.5°.

(3) Comparing water contact angles and water adhesion on polymer films across the ProDOT series, showed that these properties are mainly dominated by total carbon number in the monomer side chains $N_{c,total}$ (**Figure 6**) rather than fluorination level, branching or length of the side chains (**Figures S1 and S2**). The relationship between those properties and chemical structure of the polymers showed that as $N_{c,total}$ increases from 0 to 8 the water contact angle

increased from $\sim 90^\circ$ to 160° whilst maintaining strong water adhesion (Petal effect), changing to $\sim 160^\circ$ and ultra-low water adhesiveness (Lotus effect) at $N_{c,\text{total}} > 8$. Hence, $N_{c,\text{total}} = 8$ represents a critical cut-off for control over water adhesion (Petal or Lotus) and superhydrophobicity. The value $N_{c,\text{total}} \geq 8$ is presumably needed to achieve two important requirements for the Lotus effect, both $Ra > 290$ nm and $\theta_w^{\text{Smooth}} > 90^\circ$.

By adjusting the number of TMS groups and $N_{c,\text{total}}$, the nanofiber sizes, surface roughness and also the resulting wetting properties could be controlled, to obtain high θ_w and strong water adhesion or ultra-low water adhesion. These new results are very promising for various applications, such as water harvesting systems, liquid transportation or separation membranes, especially due to the control over water adhesion. Although polymer films with ProDOTSiMe₃ exhibited strong water adhesion, superhydrophobicity was not observed. The relationship between Ra and $(\theta_w - \theta_w^{\text{Smooth}})$ as reported in **Figure 7** indicates parahydrophobicity with $\theta_w > 150^\circ$ to appear with appropriate surface chemistry and structure for Petal and Lotus effects, in other words, $Ra = \sim 290$ nm and $\theta_w^{\text{Smooth}} = \sim 90^\circ$. From this point of view, parahydrophobicity with $\theta_w > 150^\circ$ may be generated with Ra approaching to ~ 290 nm, with ProDOTSiMe₃ and variation of solvent, temperature, additive concentration etc.

Unfortunately, superoleophobicity was not observed for the polymer films prepared in this study, even after employing single and double TMS-terminated substituents. Future work will explore optimal F-free substituent structures for ProDOTs to generate superoleophobic electrodeposited films. This is expected because even fluorinated ProDOT often leads to low oleophobicity, which could be increased by using more polar monomers such as 3,4-propylenedioxyppyrole (ProDOP) or with extra polymer linkers [46,48 49]. Such advanced polymer films could be key for applications such as self-cleaning solar panels and windows.

CRedit authorship contribution statement

D. Arisawa : Investigation, Y. Umetsu : Investigation, A. Yoshizawa : Methodology, C. Hill : Writing - review & editing, J. Eastoe : Writing - review & editing, F. Guittard : Conceptualization, Supervision, T. Darmanin: Investigation, Writing - original draft, M. Sagisaka : Supervision, Writing - original draft, review & editing

Declaration of Competing Interest

None.

Acknowledgment

The group thanks Christelle Boscagli from the Centre Commun de Microscopie Appliquée (CCMA, Université Côte d'Azur) for the preparation of the substrates necessary for the SEM analyses. This work has been supported by CNRS GDR 2088 « BIOMIM ». This project was supported by JSPS [KAKENHI, Grant-in-Aid for Scientific Research (B), No. 19H02504, Fostering Joint International Research (A), No. 15KK0221, Grant-in-Aid for Challenging Research (Exploratory), No.17K19002], and Leading Research Organizations (RCUK [through EPSRC EP/I018301/1], ANR [13-G8ME-0003]) under the G8 Research Councils Initiative for Multilateral Research Funding–G8-2012. The authors acknowledge Shared Facility Center for Science and Technology, Hirosaki University (SFCST) for ¹H-NMR and FT-IR spectra measurements and elemental analysis.

Appendix A. Supplementary data

References

- [1] T. Darmanin, F. Guittard Superhydrophobic and superoleophobic properties in nature, *Mater. Today* 18 (2015) 273–285. <https://doi.org/10.1016/j.mattod.2015.01.001>.
- [2] L. Feng, Y. Zhang, J. Xi, Y. Zhu, N. Wang, F. Xia, L. Jiang, Petal Effect: A Superhydrophobic State with High Adhesive Force, *Langmuir* 24 (2008) 4114–4119. <https://doi.org/10.1021/la703821h>.
- [3] L. Ge, S. Sethi, L. Ci, P. M. Ajayan, A. Dhinojwala, Carbon nanotube-based synthetic gecko tapes, *Proc. Natl. Acad. Sci. U.S.A.* 104 (2007) 10792–10795. <https://doi.org/10.1073/pnas.0703505104>.
- [4] B. Su, Y. Tian, L. Jiang, Bioinspired Interfaces with Superwettability: From Materials to Chemistry, *J. Am. Chem. Soc.* 138 (2016) 1727–1748. <https://doi.org/10.1021/jacs.5b12728>.
- [5] F. Guo, Q. Wen, Y. Peng, Z. Guo, Simple One-Pot Approach Toward Robust and Boiling-Water Resistant Superhydrophobic Cotton Fabric and the Application in Oil/Water Separation, *J. Mater. Chem. A* 5 (2017) 21866–21874. <https://doi.org/10.1039/C7TA05599D>.
- [6] M.J. Nine, S. Kabiri, A.K. Sumona, T.T. Tung, M.M. Moussa, D. Losic, Superhydrophobic/superoleophilic natural fibres for continuous oil-water separation and interfacial dye-adsorption, *Sep. Purif. Technol.* 233 (2020) 116062. <https://doi.org/10.1016/j.seppur.2019.116062>.
- [7] R. N. Wenzel, Resistance of solid surfaces to wetting by water, *Ind. Eng. Chem.* 28 (1936) 988–994. <https://doi.org/10.1021/ie50320a024>.

- [8] A. B. D. Cassie, S. Baxter, Wettability of porous surfaces, *Trans. Faraday Soc.* 40 (1944) 546–551. <https://doi.org/10.1039/TF94444000546>.
- [9] A. Marmur, The Lotus Effect: Superhydrophobicity and Metastability, *Langmuir* 20 (2004) 3517–3519. <https://doi.org/10.1021/la036369u>.
- [10] A. Marmur, From Hydrophilic to Superhydrophobic: Theoretical Conditions for Making High-Contact-Angle Surfaces from Low-Contact-Angle Materials, *Langmuir* 24 (2008) 7573–7579. <https://doi.org/10.1021/la800304r>.
- [11] B. Bhushan, M. Nosonovsky, The Rose Petal Effect and The Modes of Superhydrophobicity, *Phil. Trans. R. Soc. A* 368 (2010) 4713–4728. <https://doi.org/10.1098/rsta.2010.0203>.
- [12] J. Song, Z. Liu, X. Wang, H. Liu, Y. Lu, X. Deng, C. J. Carmalt, I. P. Parkin, High-efficiency bubble transportation in an aqueous environment on a serial wedge-shaped wettability pattern, *J. Mater. Chem. A* 7 (2019) 13567–13576. <https://doi.org/10.1039/C9TA02095K>.
- [13] Z. Liu, H. Zhang, Y. Han, L. Huang, Y. Chen, J. Liu, X. Wang, X. Liu, S. Ling, Superaerophilic wedge-shaped channels with precovered air film for efficient subaqueous bubbles/et transportation and continuous oxygen supplementation, *ACS Appl. Mater. Interfaces* 11 (2019) 23808–23814. <https://doi.org/10.1021/acsami.9b08085>.
- [14] H. Dai, C. Gao, J. Sun, C. Li, N. Li, L. Wu, Z. Dong, L. Jiang, Controllable high - speed electrostatic manipulation of water droplets on a superhydrophobic surface, *Adv. Mater.* 31 (2019) 1905449. <https://doi.org/10.1002/adma.201905449>.
- [15] A. Marmur, Hydro- hygro- oleo- omni-phobic? Terminology of wettability classification, *Soft Matter* 8 (2012) 6867–6870. <https://doi.org/10.1039/C2SM25443C>.

- [16] J. Yong, Q. Yang, C. Guo, F. Chen, X. Hou, A review of femtosecond laser-structured superhydrophobic or underwater superoleophobic porous surfaces/materials for efficient oil/water separation, *RSC Adv.* 9 (2019) 12470-12495. <https://doi.org/10.1039/C8RA10673H>.
- [17] K. Ellinas, A. Tserepi, E. Gogolides, From superamphiphobic to amphiphilic polymeric surfaces with ordered hierarchical roughness fabricated with colloidal lithography and plasma nanotexturing, *Langmuir* 27 (2011) 3960–3969. <https://doi.org/10.1021/la104481p>.
- [18] Z. Xue, M. Liu, L. Jiang, Recent developments in polymeric superoleophobic surfaces, *J. Polym. Sci., Part B: Polym. Phys.* 50 (2012) 1209-1224. <https://doi.org/10.1002/polb.23115>.
- [19] Q. Cheng, M. Li, F. Yang, M. Liu, L. Li, S. Wang, L. Jiang, An underwater pH-responsive superoleophobic surface with reversibly switchable oil-adhesion, *Soft Matter* 8 (2012) 6740-6743. <https://doi.org/10.1039/C2SM25421B>.
- [20] Y. Pan, W. Kong, B. Bhushan, X. Zhao, Rapid, ultraviolet-induced, reversibly switchable wettability of superhydrophobic/superhydrophilic surfaces, *Beilstein J. Nanotechnol.* 10 (2019) 866–873. <https://doi.org/10.3762/bjnano.10.87>.
- [21] D. Kim, J. Seo, S. Shin, S. Lee, K. Lee, H. Cho, W. Shim, H.-B.-R. Lee, T. Lee, Reversible liquid adhesion switching of superamphiphobic Pd-decorated Ag dendrites via gas-induced structural changes, *Chem. Mater.* 27 (2015) 4964–4971. <https://doi.org/10.1021/acs.chemmater.5b01038>.

- [22] B. T. W. Ang, J. Zhang, G. J. Lin, H. Wang, W. S. V. Lee, J. Xue, Enhancing Water Harvesting through the Cascading Effect, *ACS Appl. Mater. Interfaces* 11 (2019) 27464–27469. <https://doi.org/10.1021/acsami.9b08460>.
- [23] D. Zhang, F. Chen, Q. Yang, J. Yong, H. Bian, Y. Ou, J. Si, X. Meng, X. Hou, A Simple Way To Achieve Pattern-Dependent Tunable Adhesion in Superhydrophobic Surfaces by a Femtosecond Laser, *ACS Appl. Mater. Interfaces* 4 (2012) 4905–4912. <https://doi.org/10.1021/am3012388>.
- [24] Z. Liu, X. Yang, G. Pang, F. Zhang, Y. Han, X. Wang, X. Liu, L. Xue, Temperature-based adhesion tuning and superwettability switching on superhydrophobic aluminum surface for droplet manipulations, *Surf. Coat. Technol.* 375 (2019) 527-533. <https://doi.org/10.1016/j.surfcoat.2019.07.041>.
- [25] H. Fan, J. Wang, Q. Zhang, Z. Jin, Tannic Acid-Based Multifunctional Hydrogels with Facile Adjustable Adhesion and Cohesion Contributed by Polyphenol Supramolecular Chemistry, *ACS Omega* 2 (2017) 6668–6676. <https://doi.org/10.1021/acsomega.7b01067>.
- [26] Y. Zhao, J. Stejskal, J. Wang, Towards directional assembly of hierarchical structures: aniline oligomers as the model precursors, *Nanoscale* 5 (2013) 2620-2626. <https://doi.org/10.1039/C3NR00145H>.
- [27] S.-C. Luo, J. Sekine, B. Zhu, H. Zhao, A. Nakao, H.-h. Yu, Polydioxythiophene Nanodots, Nonowires, Nano-Networks, and Tubular Structures: The Effect of Functional Groups and Temperature in Template-Free Electropolymerization, *ACS Nano* 6 (2012) 3018–3026. <https://doi.org/10.1021/nn300737e>.

- [28] A. Diouf, T. Darmanin, S. Y. Dieng, F. Guittard, Superhydrophobic (low adhesion) and parahydrophobic (high adhesion) surfaces with micro/nanostructures or nanofilaments, *J. Colloid Interface Sci.* 453 (2015) 42-47. <https://doi.org/10.1016/j.jcis.2015.04.046>.
- [29] J. El-Maiss, T. Darmanin, F. Guittard, Low bioaccumulative materials for parahydrophobic nanosheets with sticking behaviour, *J. Colloid Interface Sci.* 447 (2015) 167–172. <https://doi.org/10.1016/j.jcis.2014.10.016>.
- [30] T. Darmanin, C. Mortier, J. Eastoe, M. Sagisaka, F. Guittard, Sticky superhydrophobic hard nanofibers from soft matter, *RSC Adv.* 4 (2014) 35708–35716. <https://doi.org/10.1039/C4RA05150E>.
- [31] C. Mortier, T. Darmanin, F. Guittard, Parahydrophobic surfaces made of intrinsically hydrophilic PProDOT nanofibers with branched alkyl chains, *Adv. Eng. Mater.* 16 (2014) 1400–1405. <https://doi.org/10.1002/adem.201400212>.
- [32] D. M. Welsh, L. J. Kloeppner, L. Madrigal, M. R. Pinto, B. C. Thompson, K. S. Schanze, K. A. Abboud, D. Powell, J. R. Reynolds, Regiosymmetric Dibutyl-Substituted Poly(3,4-propylenedioxythiophene)s as Highly Electron-Rich Electroactive and Luminescent Polymers, *Macromolecules* 35 (2002) 6517–6525. <https://doi.org/10.1021/ma0120409>.
- [33] X. Chen, H. Liu, Z. Xu, S. Mi, J. Zheng, C. Xu, Highly Regiosymmetric Homopolymer Based on Dioxythiophene for Realizing Water-Processable Blue-to-Transmissive Electrochrome, *ACS Appl. Mater. Interfaces* 7 (2015) 11387–11392. <https://doi.org/10.1021/acsami.5b01908>.
- [34] W. S. Shin, M.-K. Kim, S.-H. Jin, Y.-B. Shim, J.-K. Lee, J. W. Lee, Y.-S. Gal, Synthesis and Characterization of Regiosymmetric Poly(3,4-propylenedioxythiophene) Derivative, *Mol. Cryst. Liq. Cryst.* 444 (2006) 129–135. <https://doi.org/10.1080/15421400500365300>.

- [35] T. Darmanin, F. Guittard, Wettability of poly(3-alkyl-3,4-propylenedioxythiophene) fibrous structures forming nanoporous, microporous or micro/nanostructured networks, *Mater. Chem. Phys.* **146** (2014) 6–11. <https://doi.org/10.1016/j.matchemphys.2013.12.026>.
- [36] J. El-Maiss, T. Darmanin, F. Guittard, Controlling electrodeposited conducting polymer nanostructures with the number and the length of fluorinated chains for adjusting superhydrophobic properties and adhesion, *RSC Adv.* **5** (2015) 37196–37205. <https://doi.org/10.1039/C5RA04945H>.
- [37] T. Darmanin, C. Mortier, F. Guittard, One-pot process to control the elaboration of non-wetting nanofibers, *Adv. Mater. Interfaces*, **2014**, *1*, 1300094/1–1300094/6. <https://doi.org/10.1002/admi.201300094>.
- [38] J. El-Maiss, T. Darmanin, E. Taffin de Givenchy, S. Amigoni, J. Eastoe, M. Sagisaka, F. Guittard, Superhydrophobic surfaces with low and high adhesion made from mixed (hydrocarbon and fluorocarbon) 3,4-propylenedioxythiophene monomers, *J. Polym. Sci., Part B: Polym. Phys.* **52** (2014) 782–788. <https://doi.org/10.1002/polb.23483>.
- [39] A. Czajka, C. Hill, J. Peach, J. C. Pegg, I. Grillo, F. Guittard, S. E. Rogers, M. Sagisaka, J. Eastoe, Trimethylsilyl hedgehogs – a novel class of super-efficient hydrocarbon surfactants, *Phys. Chem. Chem. Phys.* **19** (2017) 23869–23877. <https://doi.org/10.1039/C7CP02570J>.
- [40] N. M. Kovalchuk, M. Sagisaka, S. Osaki, M. J. H. Simmons, Superspreading performance of branched ionic trimethylsilyl surfactant Mg(AOTSiC)₂, *Colloid Surf. A* **604** (2020) 125277. <https://doi.org/10.1016/j.colsurfa.2020.125277>.

- [41] C. Hill, Y. Umetsu, K. Fujita, T. Endo, K. Sato, A. Yoshizawa, S. E. Rogers, J. Eastoe, M. Sagisaka, Design of Surfactant Tails for Effective Surface Tension Reduction and Micellization in Water and/or Supercritical CO₂, *Langmuir* 36 (2020) 14829–14840. <https://doi.org/10.1021/acs.langmuir.0c02835>.
- [41 42] D. W. Smith, S. T. Iacono, D. J. Boday, S. C. Kettwich, *Advances in Fluorine-Containing Polymers*, ACS Symposium Series; American Chemical Society: Washington, DC, 2012.
- [42 43] B. Bhushan, Bioinspired water collection methods to supplement water supply, *Phil. Trans. R. Soc. A* 377 (2019) 20190119. <https://doi.org/10.1098/rsta.2019.0119>.
- [43 44] R. Gimenez, M. G. Bellino, C. L. A. Berli, Directional Water Collection in Nanopore Networks, *ACS Omega* 3 (2018) 16040–16045. <https://doi.org/10.1021/acsomega.8b02376>.
- [44 45] X. Li, Y. Yang, L. Liu, Y. Chen, M. Chu, H. Sun, W. Shan, Y. Chen, Water Collection: 3D - Printed Cactus - Inspired Spine Structures for Highly Efficient Water Collection, *Adv. Mater. Interfaces* 7 (2020) 1901752. <https://doi.org/10.1002/admi.202070012>.
- [45 46] M. Liu, Z. Peng, Y. Yao, Y. Yang, S. Chen, Flexible Functional Surface for Efficient Water Collection, *ACS Appl. Mater. Interfaces* 12 (2020) 12256–12263. <https://doi.org/10.1021/acsami.9b20222>.
- [46 47] C. Mortier, T. Darmanin, F. Guittard, Direct electrodeposition of superhydrophobic and highly oleophobic poly(3,4-ethylenedioxyppyrole) (PEDOP) and poly(3,4-propylenedioxyppyrole) (PProDOP) nanofibers, *ChemNanoMat* 3 (2017) 885–894. <https://doi.org/10.1002/cnma.201700236>.

- [47 48] M. Sagisaka, T. Narumi, M. Niwase, S. Narita, A. Ohata, C. James, A. Yoshizawa, E. T. de Givenchy, F. Guittard, S. Alexander, J. Eastoe, Hyperbranched Hydrocarbon Surfactants Give Fluorocarbon-like Low Surface Energies, *Langmuir* 30 (2014), 6057–6063. <https://doi.org/10.1021/la501328s>.
- [48 49] T. Darmanin, F. Guittard, Superoleophobic surfaces with short fluorinated chains?, *Soft* 9 (2013) 5982–5990. <https://doi.org/10.1039/C3SM50643F>.